Effect of curing condition on mechanical properties and durability of alkali-activated slag mortar

Liu, Chen; Wu, Haoming; Li, Zhenming; Shi, Hu; Ye, Guang

DOI
10.1016/j.conbuildmat.2024.137376

Publication date
2024

Document Version
Final published version

Published in
Construction and Building Materials

Citation (APA)
Liu, C., Wu, H., Li, Z., Shi, H., & Ye, G. (2024). Effect of curing condition on mechanical properties and durability of alkali-activated slag mortar. *Construction and Building Materials*, *439*, Article 137376. https://doi.org/10.1016/j.conbuildmat.2024.137376

Construction and Building Materials 439 (2024) 137376

Contents lists available at ScienceDirect

Construction and Building Materials

journal homepage: www.elsevier.com/locate/conbuildmat

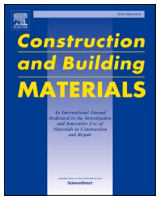

Effect of curing condition on mechanical properties and durability of alkali-activated slag mortar

Chen Liu [a], Haoming Wu [a], Zhenming Li [b,c,*], Hu Shi [a], Guang Ye [a,**]

[a] Department of Materials and Environment (Microlab), Faculty of Civil Engineering and Geoscience, Delft University of Technology, 2628 CN Delft, the Netherlands
[b] School of Civil and Environmental Engineering, Harbin Institute of Technology, 518055 Shenzhen, China
[c] Guangdong Provincial Key Laboratory of Intelligent and Resilient Structures for Civil Engineering, Harbin Institute of Technology, 518055 Shenzhen, China

ARTICLE INFO

Keywords:
Alkali-activated slag
Curing
Elastic modulus
Shrinkage
Carbonation
Freeze and thaw

ABSTRACT

While alkali-activated slag (AAS) has emerged as a promising alternative binder in construction engineering, a consensus on the optimal curing condition for this material has not been reached yet. It is well known that AAS can harden at ambient temperatures, but the influence of humidity on its properties remains poorly understood. Herein, we considered five curing conditions with different relative humidities (RH), including ambient/dry condition (RH=55 %), sealed condition (RH=80–95 %), fog condition (RH>95 %), water immersion condition (RH=100 %), and saturated limewater immersion condition (RH=100 %). Various properties have been examined, including flexural and compressive strengths, elastic modulus, shrinkage, pore structure, carbonation resistance, and freeze-thaw resistance of AAS mortars (AASM). Two types of activators, sodium hydroxide and sodium silicate (modulus at 1) solutions were used. The experimental results indicate that drying at early ages is detrimental to almost all the properties investigated. Sealed curing can deliver desirable mechanical properties and durability, but considerable shrinkage. Fog and water curings are highly effective at mitigating early shrinkage in AASM, but the problem of leaching adversely affects its long-term properties. Generally, limewater curing offers limited benefits compared to other high-humidity curing methods.

1. Introduction

As sustainable alternatives to traditional Portland cement, alkali-activated materials (AAMs) have attracted considerable attention from both academia and industry sectors in recent decades. Slag, derived from the byproducts of the metallurgy industry, stands out as one of the most commonly used precursors in AAMs. Due to its desirable hydraulic and pozzolanic reactivities, alkali-activated slag concrete (AASC) has demonstrated equivalent or even superior performance in areas such as strength development, chemical resistance and thermal stability when compared to traditional concrete [1–3]. Nevertheless, this innovative cement substitute comes with certain drawbacks, including notable issues related to shrinkage [4], low carbonation resistance [5,6], and a heightened risk of leaching [7] and efflorescence [8]. Numerous researchers are dedicated to elucidating the mechanisms behind these limitations and exploring effective mitigating strategies [9–11]. However, the critical importance of early-age curing regimes in affecting the material's long-term performance has not gained enough attention [12,13]. An inappropriate curing regime may lead to heightened permeability, extensive shrinkage and reduced mechanical properties [14,15]. Furthermore, due to the absence of standardized curing protocols for AAMs, researchers and end users tend to apply curing methods designed for ordinary Portland cement (PC) systems. However, the chemistry of PC and AAS systems varies significantly. A customized and specifically tailored curing regime is imperative for AAS materials. Historically, attempts have been made to address these challenges through various approaches.

In earlier publications, water curing was initially conducted in AAS materials. Collins et al. [15] conducted a study comparing the 1-year compressive strength of AASC cured under ambient (23°C, 50 % RH), bath (23°C, saturated limewater), and sealed (23°C) conditions. The results showed that immersion in limewater resulted in the highest compressive strength, followed by sealed curing, while samples exposed to a relatively dry environment exhibited the lowest compressive strength. Rostami et al. [16] studied the impact of water curing and plastic cover curing on the compressive strength and water absorption of

* Corresponding author at: School of Civil and Environmental Engineering, Harbin Institute of Technology, 518055 Shenzhen, China.
** Corresponding author.
E-mail addresses: zhenmingli@hit.edu.cn (Z. Li), G.Ye@tudelft.nl (G. Ye).

https://doi.org/10.1016/j.conbuildmat.2024.137376
Received 26 April 2024; Received in revised form 8 June 2024; Accepted 4 July 2024
Available online 8 July 2024

AASC blended with silica fume. Their findings were similar to [15] and further demonstrated that external water supply contributed to a higher compressive strength, lower permeability, and higher durability. Several other studies reported that high temperatures combined with high humidity are advantageous for achieving increased strength, reduced drying shrinkage, and enhanced thermal and sulfate resistance [17–21], probably because extra water supply can effectively mitigate the large shrinkage of AAS materials at early stages and reduce the cracking potential.

However, an increasing number of researchers claimed that high-humidity conditions, e.g. fog or soak curing, were seemingly not appropriate for AAS materials. The compressive strength and pore solution alkalinity of AAS binders after water immersion were lower than those in sealed condition [22,23]. In a recent publication [7], a more comprehensive overview was provided on the potential degradation of AAS pastes exposed to tap water. The study elucidated the underlying mechanisms responsible for the leaching-induced degradation, such as the reduced formation of reaction products, decomposition of gel, and carbonation. El-Hassan et al. [24] applied a so-called "intermittent water curing" (7 days in water + 21 days in open air) to AASC, and found that the samples cured in this regime exhibited superior performance in terms of compressive strength and elastic modulus compared to those solely exposed to air or immersed in water.

Thus far, the knowledge on how different curing regimes impact the performance of AAS is insufficient to establish a standardized curing protocol for AAS materials. To fill this gap, five curing regimes including ambient/dry condition (RH=55 %), sealed condition (RH=90–95 %, as illustrated in **Fig. A1**), fog condition (RH>95 %), water condition (RH=100 %), and limewater condition (RH=100 %, saturated $Ca(OH)_2$ solution) were adopted to cure sodium hydroxide- and/or sodium silicate-activated slag mortars. Mechanical properties (compressive strength, flexural strength and elastic modulus), shrinkage, pore structure, water sorptivity, carbonation and freeze-thaw resistance of AASM cured under these conditions were investigated. The results of this work contribute to the understanding of the influence of moisture on the AAS materials at curing periods. Hopefully, it is valuable for academic research and engineering practice to identify suitable curing protocols for AAS materials.

2. Materials and methods

2.1. Raw materials and mixture design

The chemical composition of slag was determined using X-ray fluorescence (XRF), as presented in Table 1. The particle size distribution of the slag was measured using a laser diffraction analyzer, which indicated a d_{50} value (medium particle size) of 17.88 μm. The particle size of sand ranged from 0 mm to 4 mm.

LOI: loss on ignition

Slag was activated by sodium hydroxide (NH) and/or sodium silicate (NS) solutions. The NH activator was prepared by diluting 50 wt.% NaOH solution with water and the NS activator was prepared by combining commercial water glass solution (consisting of 8.25 g Na_2O, 27.5 g SiO_2, and 64.25 g water per 100 g solution) with a 50 wt.% NaOH solution and additional water. The alkali dosage (Na_2O) of the two activators remained constant at a moderate dosage of 5 % according to [7]. The mixture design of AASM is shown in Table 2. The sand was first added in a mixer followed by slag, which was mixed for 1 min. Afterwards, the activator was poured into the mixing bowl. The slurry was blended for 1 min at a low-speed rate and another 1 min at a high-speed rate. The entire casting process was performed in an indoor environment at 20°C and a RH of 55 %. Fresh mortars were cast into three types of moulds for different measurements: 40 mm × 40 mm × 160 mm (strength, elastic modulus, shrinkage, freeze-thaw and carbonation), φ 100 mm × 200 mm (water sorptivity) and small polyethene cylinder bottles (pore structure characterization). The mortars were sealed for 1 day before demolding. Afterwards, the specimens were cured in 5 different conditions: ambient curing (a), sealed curing (s), fog curing (f), water curing (w), and saturated limewater curing (l) for designed days. For example, the mixture termed as "NH_a" means NH-activated slag cured in ambient condition after demoulding.

Table 2
Mixture design of AASM.

	slag (g)	Na_2SiO_3 (g)	NaOH (g)	water (g)	w/b	sand (g)
NH	1000	0	64	490.6	0.5	2500
NS	1000	174.5	45.4	382.6	0.5	2500

w/b refers to the water/slag ratio.

2.2. Experiments

2.2.1. Flexural strength

The 40 mm × 40 mm × 160 mm samples at the ages of 7, 28 and 90 d were used for the flexural strength test at a loading rate of 50 N/s. The detailed procedures were according to EN196–1 [25]. Three replicates were measured for each mixture under each condition.

2.2.2. Compressive strength

After completion of the flexural strength, six halves of specimens at 7, 28 and 90 d were obtained for each mixture and subjected to the compressive strength test. The loading rate was 2.4 kN/s. The detailed procedures were followed by [25].

2.2.3. Elastic modulus

The elastic modulus of AASM at 7, 28 and 90 d was performed on a servo-hydraulic testing machine (Instron® 8872) according to [26]. Four linear variable differential transformers (LVDTs) were attached to each side of the prismatic specimen (40 × 40 × 160 mm) with a span of 10 cm. A load control at a rate of 0.1 kN/s was applied to measure the modulus of elasticity and 3 loading cycles were conducted after preloading.

2.2.4. Shrinkage

The volume change of AASM under different curing conditions was measured, according to ASTM C596 [27]. The samples after demolding (1 d) were cured under the five conditions. The change in length and weight of prisms was continuously measured at 1, 2, 3, 4, 6, 7, 9, 11, 14, 17, 21, 24, 28, 36, 42, 56 and 91 d. After gauging, the samples would be restored to the place they belonged to.

2.2.5. Pore structure characterization

Mercury intrusion porosimetry (MIP) was conducted using a Micrometrics PoreSizer with a maximum intrusion pressure of 210 MPa to characterize the pore structure of AASM. The cylinder samples (prepared in the small polyethene bottle as mentioned in Section 2.2) cured in different conditions for 28 days were crushed into small pieces (4–6 mm) and then immersed in isopropanol to stop the reaction. After 7 days of reaction arresting, the samples were stored in a vacuum freeze dryer. Characterization was not conducted until they reached constant

Table 1
Chemical composition of slag (%).

	CaO	Al_2O_3	SiO_2	MgO	Fe_2O_3	SO_3	K_2O	TiO_2	other	LOI
Slag	38.28	13.9	32.19	9.52	0.31	1.52	0.51	1.27	1.17	1.33

weights.

2.2.6. Water sorptivity

Capillary pores enable external water or vapour to infiltrate and migrate through interconnected pathways within the matrix. The water sorptivity test was performed to evaluate the open capillary pore content and pore connectivity of the material [28–30]. It also serves as a crucial criterion for assessing the resistance to harmful ions [31]. The water sorptivity of AASM was assessed according to ASTM C1585 [32]. The specimens were cured in five conditions for 28 days and were then moved to a climate chamber at a temperature of 50 ± 2°C and a RH of 80 ± 3 % for 3 days. Then, the specimens were sealed in a container at 20 ± 1°C for 14 days. After preconditioning (3 d + 14 d), all side and top surfaces were sealed using aluminium tapes. During the test, the specimens were placed on a plastic mesh resting at the bottom of a container, with a water depth of 2 mm. The mass increment of samples was recorded at specific testing intervals: 60 s, 5 min, 10 min, 20 min, 30 min, 60 min, 6 h, 1 d, 2 d, 3 d, 4 d, 5 d, 6 d, 7 d, and 9 d. Three replicates were measured for each mixture under each condition. The water sorptivity I (mm) of specimens was calculated using Eq. 1:

$$I = \frac{m_t}{S \times \rho} \quad (1)$$

Where m_t (g) is the mass of samples at day t, S (mm^2) is the exposed area of the cylinder sample, ρ (10^{-3} g/mm^3) is the density of water.

2.2.7. Freeze and thaw resistance

A modified capillary suction of deicing solution and freeze-thaw test (CDF) test in accordance with [33] was performed to assess the freeze-thaw resistance of AASM. The prismatic samples after 28 days of curing were placed in an ambient environment (T=20°C and RH=55 %) for 7 days as pre-treatment. The weight change during this procedure was monitored and remained below 1 % until 7 days. After that, the side surfaces of the specimens were covered by aluminium foil glued with butyl rubber and a 7-day pre-saturation by capillary suction was conducted prior to CDF test. Finally, six replicates of each mixture were stored in the CDF containers with bottom supports, and a 3 % (by mass) sodium chloride solution was poured into the container to a height of 10 ± 2 mm above the test surface. After 4, 6, 28 freeze-thaw cycles (corresponding to 2, 3 and 14 days, respectively), the container, along with samples and liquid, was immersed in an ultrasonic bath and subjected to ultrasonic cleaning for 3 minutes. Then, the scale-off debris was carefully collected with filter paper and then dried in an oven of 105 °C for 24 h. The mass of debris was measured after cooling. Eventually, the appearance of the exposed surface after 28 CDF cycles was observed and documented. A 12 h freeze-thaw cycle was implemented. The temperature started at +20 °C, and gradually decreased over 4 h with a constant cooling rate of 10 °C /h.

2.2.8. Carbonation

An accelerated carbonation test was conducted in a CO_2 chamber (1 % v/v at 60 % RH and 20 °C [34]) to evaluate the carbonation resistance of the AASM. The samples cured in five regimes for 28 d were placed in an ambient environment with 20 °C and 55 % RH for drying precondition for another 28 d. The carbonation depth of samples at 0, 3, 7, and 28 days of accelerated carbonation was determined by spraying a phenolphthalein alcohol solution onto the freshly broken cross-sections. The value was averaged from 12 locations on each sample. Additionally, the compressive strength of AASM was measured before and after 28 days of accelerated carbonation.

3. Results and discussion

3.1. Strength

3.1.1. Flexural strength

Fig. 1 shows the flexural strength of AASM under five curing regimes. It is evident that the flexural strength of NS mortars is higher than that of NH ones regardless of the curing conditions. This is attributed to the presence of soluble Si in the sodium silicate activator, which can promote the formation of reaction products and the densification of microstructure [35]. Interestingly, two types of mortars exhibit divergent tendencies over time under different curing conditions. For the NH mortars, the samples subjected to ambient and sealed conditions exhibit lower flexural strength and show no significant change throughout 90 days of curing. In contrast, the flexural strengths of NH_f, NH_w, and NH_l groups all increase over time. This indicates that a higher relative humidity benefits NH mortars in achieving a higher long-term flexural strength. With respect to NS-activated mortars, the flexural strength decreases over time under high-humidity and ambient conditions. Sealed curing appears to be a desirable regime for NS mixtures to deliver a high early-age flexural strength as well as considerable increments with time.

Flexural strength is sensitive to microcracks and surface defects [10]. As shown in Fig. 1, ambient curing negatively impacts the development of flexural strength of both NH and NS mortars. This can be attributed to significant dry shrinkage commonly observed in AAS materials [36], which leads to the formation of micro to visible cracks (**Fig. A2**). These cracks tend to propagate under tensile stress, eventually resulting in an earlier failure of the sample. Extra water supply is normally considered efficient to mitigate shrinkage and cracking potential in cementitious materials, as it can compensate for the water loss caused by self-desiccation or drying. However, extra water supply seems to be only efficient in NH mortars. According to [7,37,38], the NS pastes show zero flexural strength after short-term immersion, and the cracking problems are more severe in the pastes with high silicate modulus. The potential mechanism is that water penetration can induce an uneven distribution of water content, which leads to an uneven distribution of internal stress [37]. The paste with a higher silicate modulus shows higher internal stress and more severe cracking problems. Fortunately, the presence of sand may help to stabilize the matrix and distribute stress more evenly, thereby mitigating the potential for cracking of NS mortars while still affecting flexural strength.

3.1.2. Compressive strength

Fig. 2 shows the compressive strength of NH and NS mortars under five curing conditions. By and large, the compressive strength of NS mortars is higher than that of NH ones. The compressive strength is predominantly reliant on the porosity of materials, and that of NS mortars is significantly lower than NH mortars (Fig. 7). Except for the NS mortar under ambient conditions, all other samples demonstrate positive correlations between compressive strength and curing duration. Additionally, both NH and NS mortars cured under sealed conditions exhibit higher compressive strength compared to those in high-humidity environments. In the case of cementitious materials, a sufficient water supply typically promotes further hydration of cement, resulting in a denser microstructure [30,39]. For AAS materials, however, alkalis are necessary for the reaction besides water. A humid atmosphere can give rise to the depletion of alkalis and hydroxyls [40], resulting in a lower reaction of slag and even the decomposition of reaction products [7]. Even though saturated limewater can provide additional calcium ions and relieve the ions loss under leaching conditions, it appears to be inefficient to increase the compressive strength.

Moreover, the NH mortar exposed to ambient conditions shows the highest compressive strength among five NH mortars (Fig. 2A), whereas the compressive strength of NS mortars under ambient regime shows a reduction from 28 d to 90 d. It is plausible that the ambient condition has

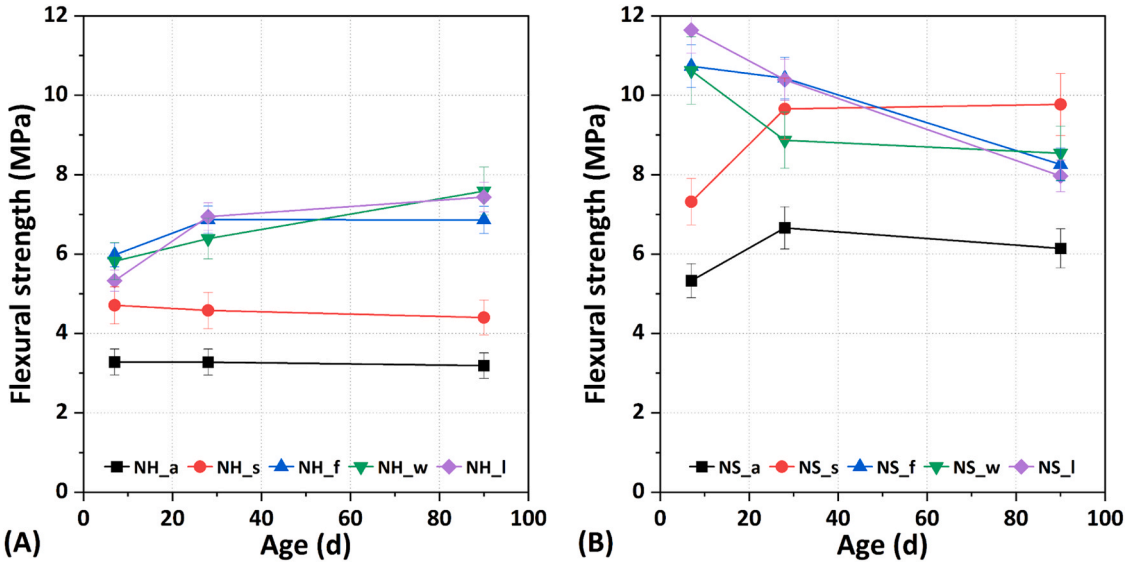

Fig. 1. Flexural strength of AASM cured under five conditions with time.

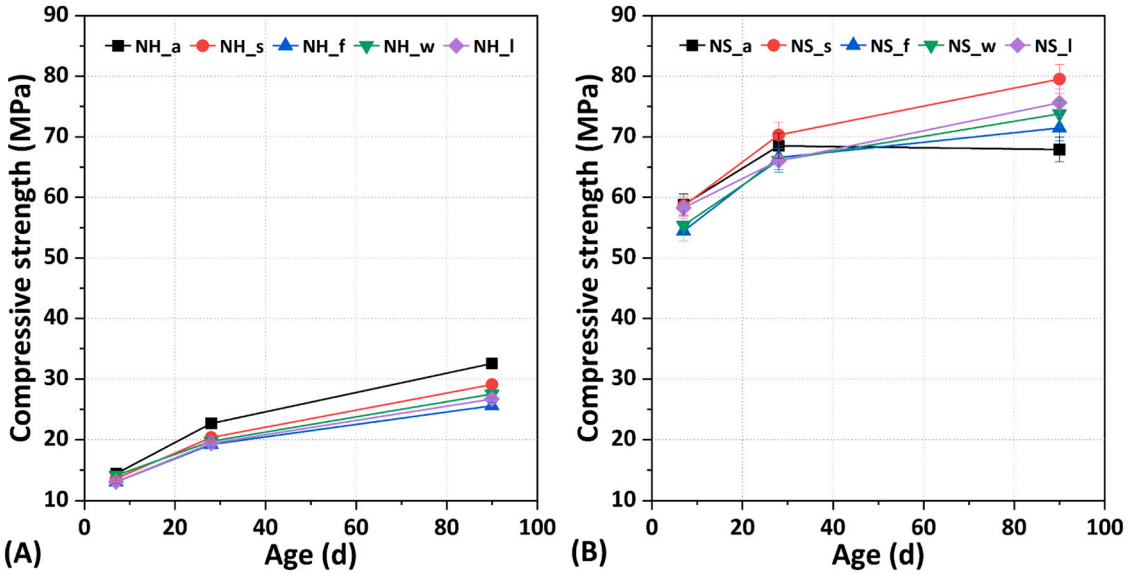

Fig. 2. Compressive strength of AASM cured under five conditions with time.

varying impacts on AASM with different moduli. This is mainly due to the presence of CO_2 in ambient conditions. Fig. 3 shows the fresh sections of samples with and without phenolphthalein spray. It can be seen that carbonation happens under ambient conditions. The NH and NS mortars after 90 days of ambient curing show similar CO_2 penetration depths, indicated by the presence of white layers, measuring approximately 8 mm.

Despite similar carbonation depths identified in both NH and NS mortars, the impact of carbonation on their microstructure is different. Shi et al. [41] also found that the NH mortar after carbonation shows a higher compressive strength than that before carbonation. They attributed this to a higher concentration of Ca in the pore solution of NH mortars, which facilitates the formation of calcium carbonation under ambient conditions [42]. The formation of calcium carbonate is a volume expansion reaction, which can densify the microstructure. However, in NS mortars, less Ca is available in the pore solution and the Ca/Si ratio of gels is also lower than in NH mortars [7]. As reported in [43], the gel with a lower Ca/Si ratio is more vulnerable to decalcification under accelerated carbonation conditions. Consequently, this leads to deteriorated microstructure and reduced compressive strength of the NS mortar after carbonation.

Interestingly, it is observed that the mortars show different extents of discolouration after exposure and the discoloured region appears not to be solely due to carbonation. According to [44], the “green effect” of AAS materials is due to the presence of sulfide-based compounds, which can be discoloured through oxidation [45]. This indicates that the diffusion coefficient of oxygen is higher than carbon dioxide in AASM. According to [46], when the pore diameter is lower than a critical value, the diffusion of gas is controlled by Knudsen diffusion. Due to a lower molecular mass of oxygen than carbon dioxide, the diffusion coefficient of oxygen is higher than that of carbon dioxide, resulting in a higher penetration depth of oxygen. Additionally, it can be seen that the oxidized region in NS mortars is larger than that in NH mortars. Knudsen diffusion occurs when the mean free path of gas molecules is comparable to or greater than the dimensions of the pores through which the molecules are diffusing. In NH mortars, the larger pores may reduce the effectiveness of Knudsen diffusion compared to NS mortars. This difference in pore structure can significantly affect the rate and extent of

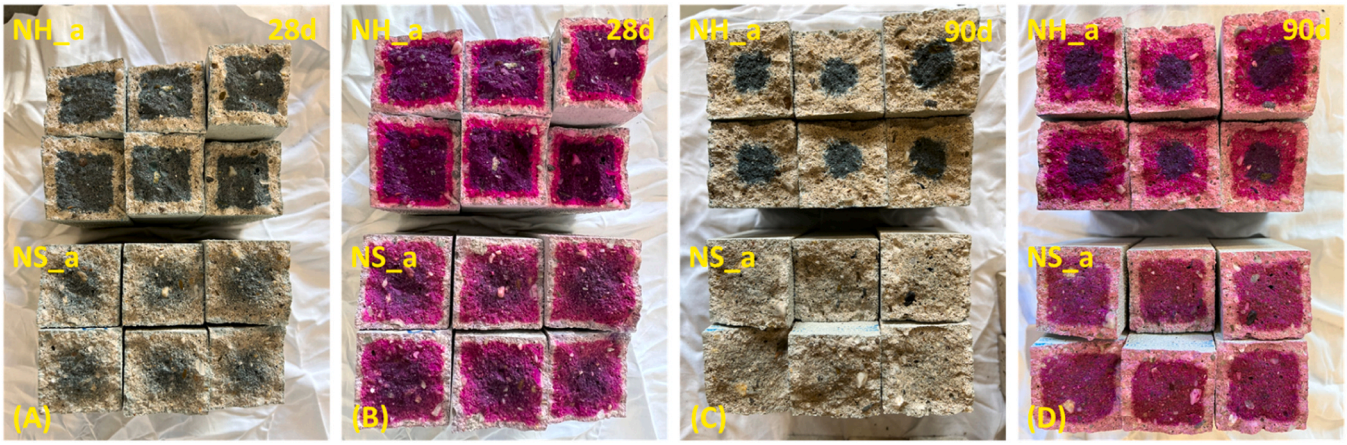

Fig. 3. Cross-section of AASM (fresh surfaces after flexural strength tests) exposed to ambient curing conditions for 28 and 90 days. (A) and (C): before phenolphthalein spraying; (B) and (D): after phenolphthalein spraying.

oxidation within the material.

3.2. Elastic modulus

Elastic modulus is dependent on the inherent mechanical property of the paste as well as the type and content of fine and coarse aggregates [47]. Fig. 4 shows the elastic modulus of AASM cured under different conditions as a function of time. Generally, the elastic modulus of NS mortars is higher than NH ones, regardless of curing conditions. This agrees with the results of flexural and compressive strengths.

As shown in Fig. 4A, the elastic modulus of NH-activated mortars increases with the increase of curing ages under all five conditions. At 90 d, the fog-cured sample shows the highest elastic modulus among all five curing regimes, followed by sealed, water, and limewater curing, while the sample subjected to ambient curing yields the lowest value. These findings indicate that high humidity is conducive to the development of elastic modulus in NH mortars. As observed in Fig. 4B, the elastic modulus of NS mortars cured under high-humidity conditions consistently increases with time. The sealed mortar reaches a plateau at 28 d and maintains that level until 90 d. Notably, the NS mortar cured under ambient conditions decreases constantly over 90 days. This decline can be attributed to the significant cracks induced by dry shrinkage (**Fig. A2**).

Fig. 5 shows the correlation between compressive strength and elastic modulus of AASM. Given a compressive load in elastic modulus tests, the results of the elastic modulus are correspondingly related to the compressive strength. Indeed, positive correlations between the elastic modulus and compressive strength can be observed in both NH- and NS-activated mortars. Due to the higher porosity of NH mortars (Fig. 7), the elastic modulus is much lower than that of NS mortars. Furthermore, it should be noted that both NH and NS mortars under ambient conditions show relatively lower elastic modulus than those with comparable compressive strength. The reduction can be ascribed to the significant drying or carbonation. However, the degradation mechanism behind NH mortars remains unclear because the compressive strength of NH mortars under ambient conditions is higher than under the other four conditions. A possible reason can lie in the decalcification of gels which leads to reduced elastic modulus.

3.3. Shrinkage

Intensive studies have reported that AAS pastes exhibit considerably higher shrinkage than Portland cement pastes [36]. Such substantial shrinkage has the potential to trigger cracking when the composites are

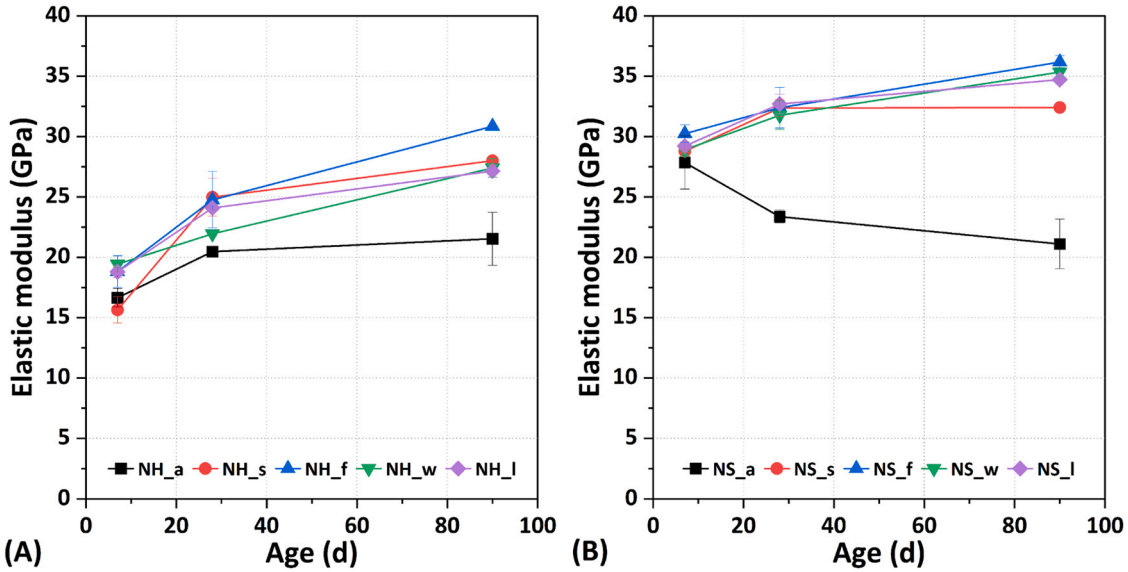

Fig. 4. Elastic modulus of AASM cured under five conditions with time.

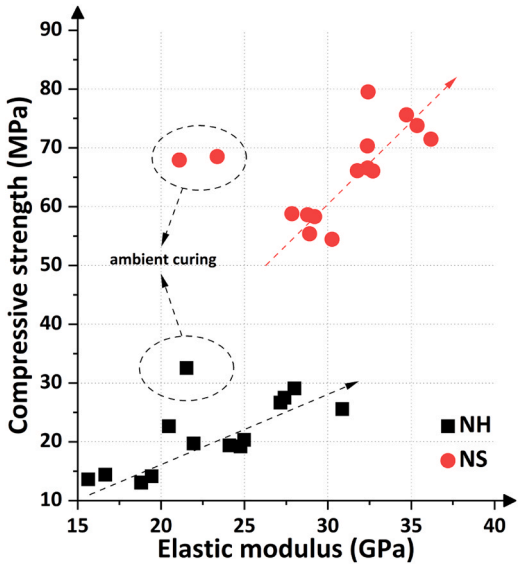

Fig. 5. Correlation between compressive strength and elastic modulus of AASM.

restrained [48]. The shrinkage and mass change of AASM cured under five conditions are shown in Fig. 6. It is observed that NH mortars have substantially lower shrinkage than NS mortars in both ambient and sealed conditions. This difference is attributed to a smaller pore size diameter (Fig. 7) and lower RH in the NS mortar [4], which can induce higher capillary pressure than that in the NH one. Curing under high-humidity conditions leads to a significantly reduced shrinkage in both NH and NS mortars since external water can compensate for the shrinkage induced by chemical reactions. However, during the first 7 days, there is still a small magnitude of shrinkage for all mixtures, which verifies the hypothesis that other shrinkage mechanisms exist besides desiccation and capillary pressure [4]. For both NH and NS mixtures, shrinkage under drying conditions is roughly twice as much as that under sealed conditions. Interestingly, there is a marginal expansion in the NH mortars at the early ages which might be attributed to the formation of crystalline phases. Generally, the critical role of moist curing in mitigating the shrinkage of AASM is evident.

Fig. 6C and D show the mass change of NH and NS mortars under the five regimes over 90 days. In high-humidity conditions, the mass of both two mortars increases with time due to the effect of capillary suction, and the increment of mass change in NS mortars appears to be higher than in NH mortars. Under moist or immersed conditions, AASM would be subjected to leaching issues [7,49]. Large amounts of Na can leach away from the materials, which probably results in the reduction of mass. Considering the porous structure of NH mortars, more Na from the

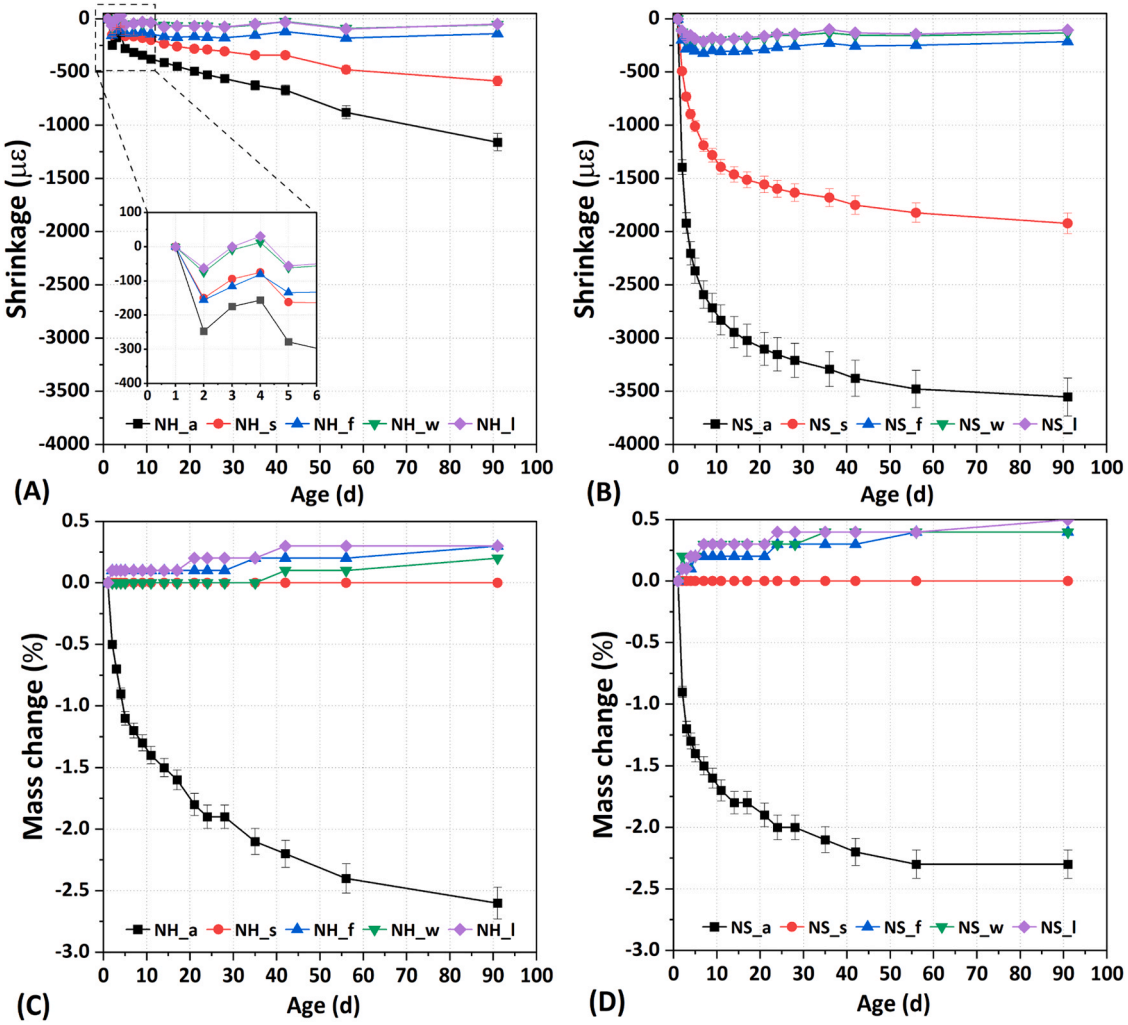

Fig. 6. Shrinkage and mass change of AASM cured under five conditions. All the mortars were sealed in the mould for 1 d and then constantly stored in five curing conditions for length and mass measurement.

pore solution and gels can leach than NS mortars. Therefore, the NS mortar obtains a higher mass increment although it has a dense microstructure. The samples kept in sealed condition maintain a constant weight over time, indicating effective sealing. Additionally, the weight loss of NH and NS mortars in the ambient condition is comparable, although the NS mortar shows larger porosity. This can be attributed to the development of microcracks in NS mortars, as shown in **Fig. A2**, which can provide moisture evaporation with additional pathways.

3.4. Pore structure

The cumulative intrusion and log differential intrusion of AASM ranging from 7 nm to 100 μm are illustrated in Fig. 7. Normally, pores in building materials can be classified by size into several types: gel pores (0–10 nm), small capillary pores (10–100 nm), large capillary pores (100–1000 nm) and air void or cracks (> 1000 nm). It is observed that the NS mortar exhibits a lower pore volume than the NH mortar. This can be attributed to the presence of soluble Si provided by the sodium silicate activator, which promotes the gelation process and compacts the microstructure. Besides, NH and NS mortars also show different pore size distributions. As shown in Fig. 7**C** and **D**, the NS mortar has a higher content of gel pores but a lower content of capillary pores than the NH mortar.

As for NH mortars, the cumulative intrusion of pores between 7 nm and 100 μm is comparable under five conditions, approximately 0.06 ml/g. The NH mortar cured under ambient conditions shows the lowest porosity, which is consistent with its highest compressive strength (Fig. 2**A**). As mentioned above, this is due to the formation of calcium carbonate under ambient conditions which can dense the porous microstructure of NH mortars [41]. Additionally, NH mortars cured under sealed and high-humidity environments show higher porosity than those under ambient conditions, especially in the pore diameter range of 10–100 nm. This indicates that the drop in pore volume of ambient-cured samples is due to the reduction in small capillary pores. As for NS mortars, the porosity of specimens under sealed and high-humidity conditions is comparable, which is lower than that under ambient conditions. This is primarily because the mortar with a high silicate modulus is more vulnerable to dry shrinkage under ambient conditions [43]. The coarsened microstructure of NS mortars upon natural carbonation is also detected in [41]. Generally, different curing conditions do not significantly influence the porosity of mortars within 28 d.

3.5. Sorptivity

Fig. 8 shows the water sorptivity behaviour of 28 d AASM over 9 days. Overall, the NS mortar has a lower water absorption rate than the NH mortar under the same curing condition, attributed to a lower porosity of NS mortars. The sorptivity of both two types of mortars cured under ambient conditions is significantly higher than under the remaining four conditions. It appears contradictory to the findings mentioned above, the NH mortar shows a higher compressive strength and a lower pore volume under ambient conditions. Given the variations in the water content of mortars subjected to different curing regimes, the high water sorptivity of mortars cured under ambient conditions is due to the low water content of the matrix, despite the preconditioning.

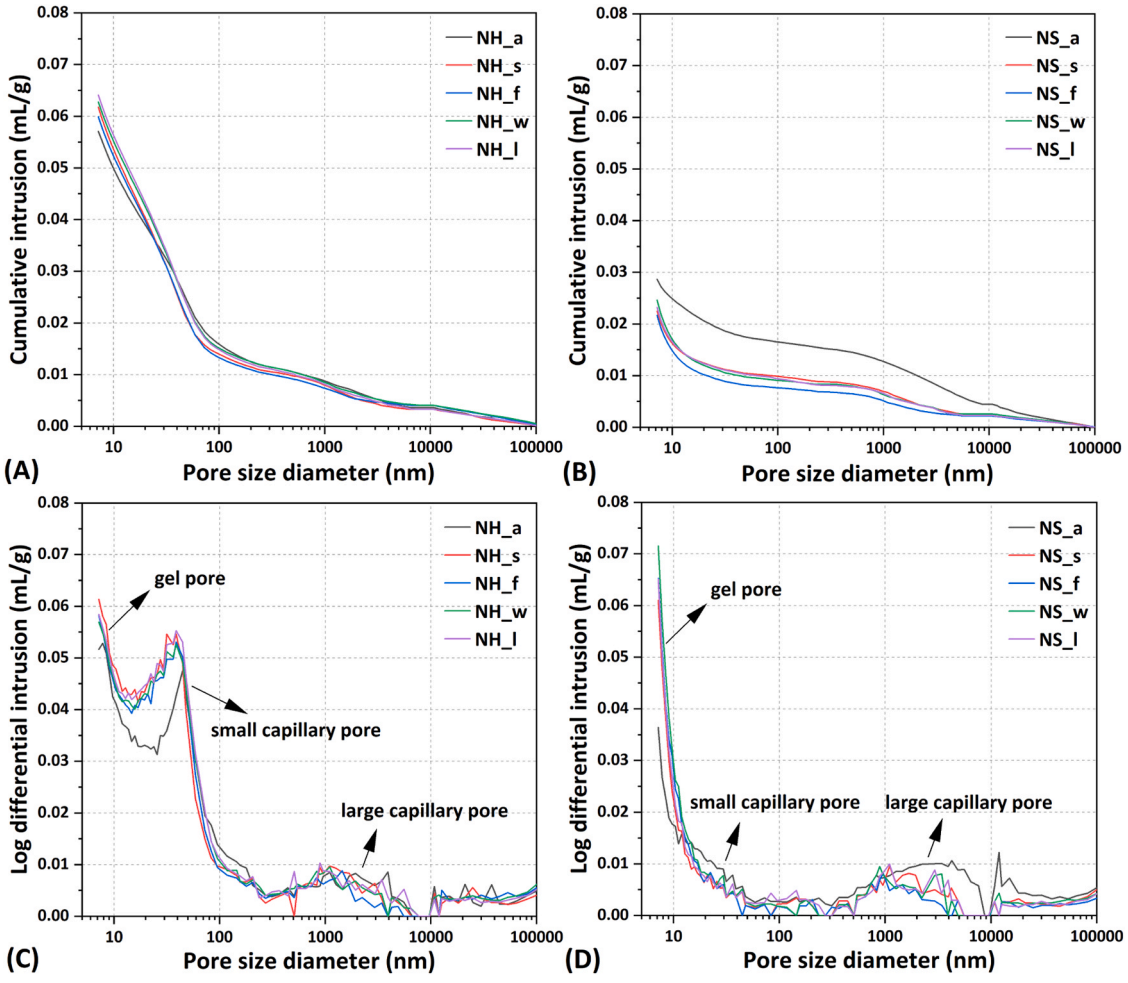

Fig. 7. Cumulative intrusion and log differential intrusion of 28 d AASM cured under five conditions ranging from 7 nm to 100 μm.

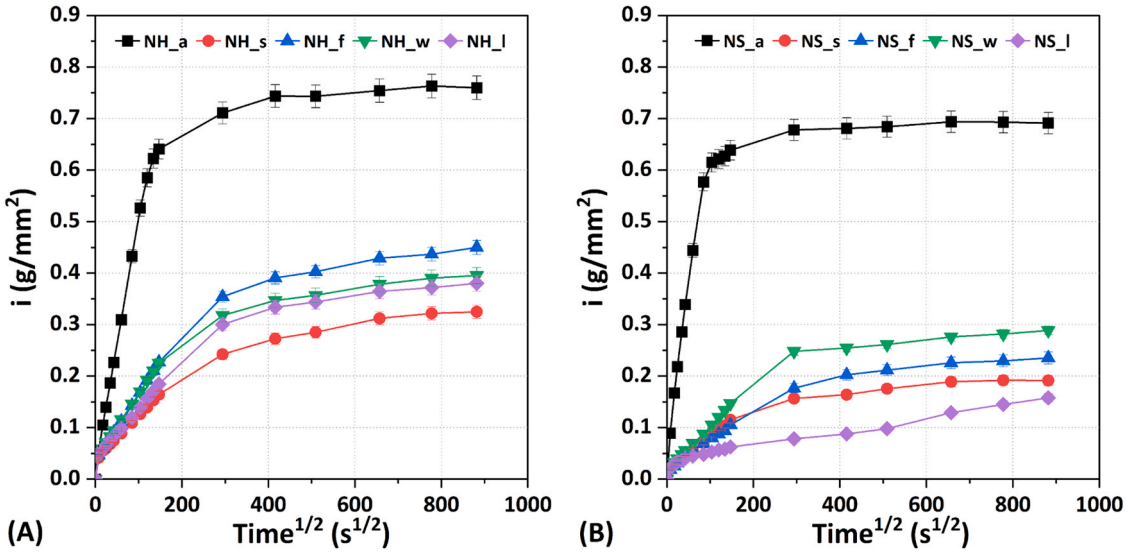

Fig. 8. Water sorptivity behaviour of 28 d AASM cured under five conditions within 9 days.

Moreover, both the NH and NS samples under sealed and limewater curings show lower water absorption than those under fog and water curings. Under high-humidity conditions, the specimens are subjected to leaching, which can degrade the microstructure of AASM [7]. Therefore, the samples under high-humidity conditions show higher water sorptivity than those under ambient conditions. However, it is plausible that the presence of calcium hydroxide can alleviate the adverse effects of leaching through the supply of additional Ca^{2+} and OH^- ions. A possible reason is that the limewater can introduce additional Ca ions to the pore solution of mortars, which results in the formation of calcium carbonation through the interaction with CO_2 during preconditioning procedures, thereby densifying the surface microstructure of mortars [50]. It is noteworthy that the positive effect of limewater curing is more pronounced in the NS system, as the Ca concentration in the pore solution of NS systems is lower than in NH systems [7].

3.6. *Freeze-thaw*

The cumulative weight loss of 28 d AASM subjected to freeze-thaw cycles is shown in Fig. 9. It is evident that the mass loss of NH mortars is much higher than that of NS mortars under the same curing age. This is primarily related to the pore structure. According to [51], the deterioration process of freeze-thaw can be described as three stages, including water absorption, water freezing, and cracking generation and propagation. Since the NH mortar is more porous than the NS one, it tends to absorb more water during preconditioning. Then, a higher amount of absorbed water can lead to increased crystallization pressure upon freezing. The exposed surface of the sample undergoes tensile stress. If this stress exceeds the tensile strength of the material, cracks will initiate and propagate throughout subsequent freeze-thaw cycles. Consequently, the NH mortar shows a poorer resistance to freeze-thaw cycles.

As shown in Fig. 9, the mass loss of AASM under ambient conditions after 28 cycles is significantly higher than that of the other four groups. The major reason is that the mortar under ambient conditions is subjected to dry and carbonation, leading to significant cracks (**Fig. A2**). The mortars with these defects have been shown to absorb more water than those under other conditions, as indicated in the sorptivity results

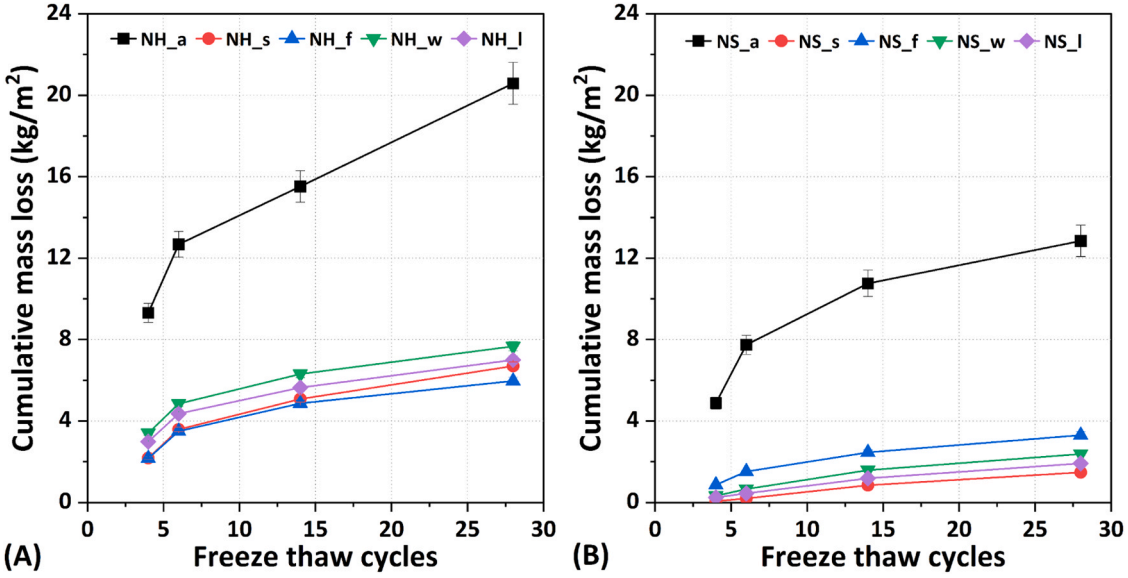

Fig. 9. Cumulative mass loss of 28 d AASM subjected to freeze-thaw cycles.

(Fig. 8). Higher water uptake can induce increased internal stress from ice formation, thereby resulting in more severe structural damage. Besides, the mortars under the remained four conditions show comparable mass loss upon 28 cycles, which is consistent with the water sorptivity results (Fig. 8). This indicates a positive relation between the water sorptivity and freeze-thaw tests.

The appearance of the top and bottom (exposed) surfaces of AASM after 28 freeze-thaw cycles is shown in Fig. 10. Notably, the testing surface of the NH mortars exhibits severe degradation after 28 freeze-thaw cycles, with the cover layer of paste scaled off and aggregates exposed. The NH mortar cured under ambient conditions shows the most severe deterioration. The top surface is damaged as well, although not totally scaled off. This is likely attributed to the thorough penetration of water into the prism, especially along the side. Actually, the standard CDF test [52] is designed for concrete cubes, with a thickness of 150 mm, while the mortar samples used in this study are 40 mm × 40 mm in width and thickness. Hence, deeper penetration of salt solution is expected. In the case of NS prisms, only the one cured under sealed conditions shows minimal damage on the bottom and top, whereas those cured under ambient and high-humidity conditions exhibit different extents of deterioration. These observations are in agreement with the results in Fig. 9.

In general, the AASM cured under sealed conditions exhibited a relatively high resistance to freeze-thaw cycles. This is likely due to the sealed samples showing fewer cracks after preconditioning (7 d drying) than the samples under ambient and high-humidity conditions. For samples under ambient curing, a continuous drying process can lead to large shrinkage and significant cracking problems. However, the samples cured under high-humidity conditions may encounter the problem of cracking during both the curing period (for NS mortars) and the preconditioning process. When the samples are exposed to ambient conditions, AASF initially with a high internal humidity will experience a more severe volume contraction due to a larger gradient of humidity. Therefore, the result of freeze-thaw is not only affected by curing methods but also the preconditioning period. In cementitious materials, 7 d of drying aims to enhance the absorption of sodium chloride solutions, seemingly without significant effects on the surface property. However, for AAMs, particularly slag-based AAMs, it is plausible that the traditionally used precondition regime for freeze-thaw tests in conventional cement and concrete requires modification in the future.

3.7. Carbonation

The carbonation depth of AASM exposed to 1 % CO_2 concentration as a function of the square root of time is shown in Fig. 11. Given that the mortars were stored in a room atmosphere with T=20 °C and RH=50 % for 28 days for preconditioning, the carbonation depth before the test was measured as well. It is observed that the mortar cured under ambient conditions already exhibits a carbonation depth of around 4 mm before being exposed to an accelerated CO_2 atmosphere. The mortars under sealed conditions show the lowest penetration depth, followed by those under high-humidity and ambient conditions. This is because the mortars under ambient conditions are subjected to cracking problems (**Fig. A2**). The diffusion of CO_2 can be promoted by the presence of cracks, thereby resulting in a higher penetration depth. In contrast, the mortars under sealed conditions show fewer cracks and less gradient of RH between the matrix and environment during preconditioning, which contributes to a lower CO_2 penetration depth before accelerated carbonation tests.

As shown in Fig. 11, the carbonation depth of mortars increases with exposure time. In spite of a much lower porosity of NS mortars than NH mortars (Fig. 7), the penetration depth of CO_2 of NS mortars is narrowly higher than that of NH mortars. There are two main reasons. On one hand, the alkalinity of the pore solution decreases with the increase of silicate modulus at the same Na_2O dosage [7]. A relatively lower pH in the NS system is unfavourable to the carbonation resistance in terms of the pore solution alkalinity. On the other hand, compared with Portland cement mortars [53,54], AASM is more susceptible to carbonation despite having a higher pore solution alkalinity. An essential reason lies in the absence of a buffering phase like $Ca(OH)_2$ in the pore solution [6]. It acts as a principal carbonatable phase, promoting the formation of calcium carbonate that provides a protective barrier against

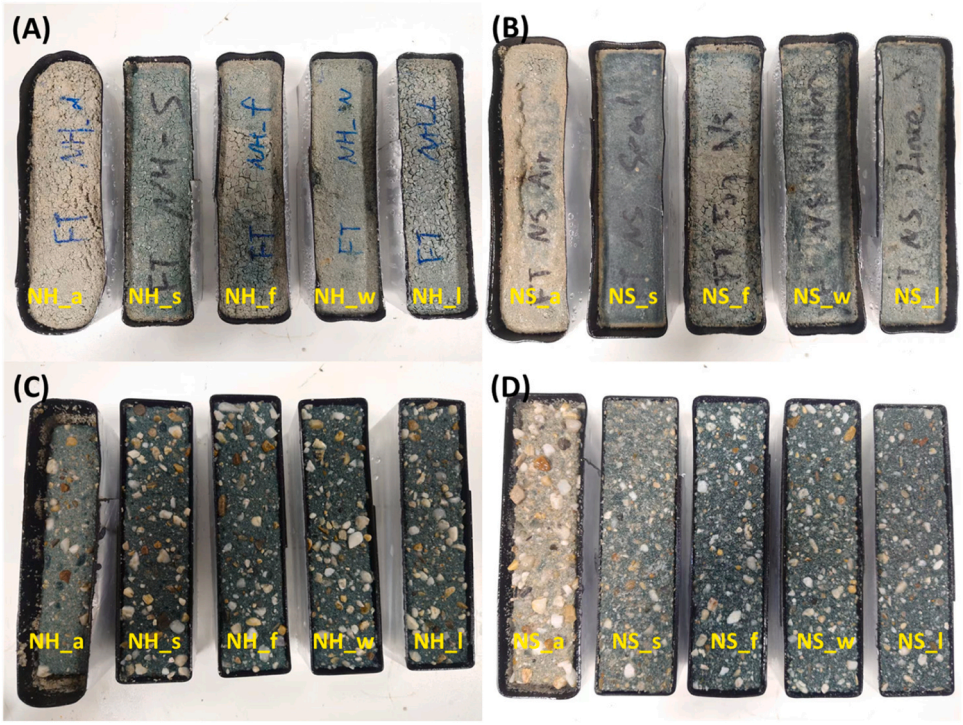

Fig. 10. Appearance of the top and bottom (exposed) surfaces of 28 d AASM after 28 freeze-thaw cycles. (A) top surfaces of NH mortars; (B) top surfaces of NS mortars; (C) exposed surface of NH mortars; (D) exposed surface of NS mortars.

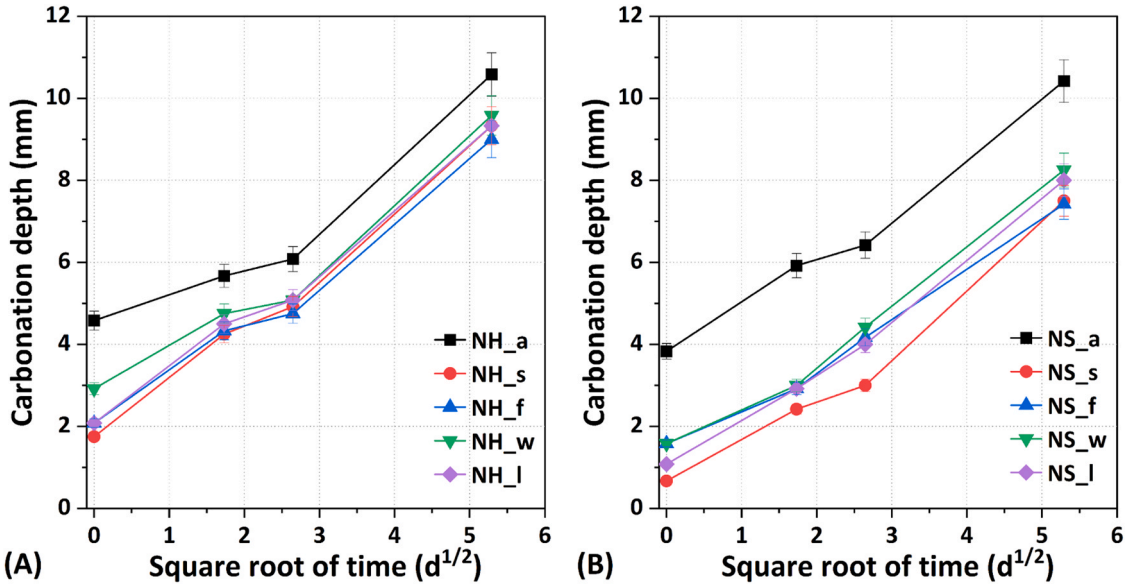

Fig. 11. Carbonation depth of 28 d AASM upon 28 d of accelerated carbonation.

carbonation. Despite the absence of calcium hydroxide in both NH and NS systems [7,41], the Ca concentration in the pore solution of the NH system is higher than that of the NS system [7]. These free Ca^{2+} ions can also contribute to the formation of calcium carbonate [41], hindering the diffusion of CO_2. In addition to the ambient curing, the carbonation depth in both NH and NS pastes under the remaining four curing conditions is comparable, respectively. Therefore, to achieve relatively good resistance to carbonation, it is recommended to avoid curing samples under ambient conditions during early periods.

Due to the initial large penetration depth before accelerated carbonation tests, the mortars under ambient conditions finally show the highest penetration depth after 28 days of exposure. However, the carbonation rates (the slope of lines) of NS_a and NH_a are not higher than those cured under other conditions, as indicated by the comparable increment of carbonation depth during the accelerated carbonation tests. This indicates that 28 days of curing and 28 days of pre-conditioning affect more on the pore structure at the external part of AASM.

The compressive strength of AASM before and after 28 days of accelerated carbonation is shown in Fig. 12. Generally, accelerated carbonation results in a reduction in compressive strength of NS mortars, whereas an increase in NH mortars. The former is due to the lower Ca/Si ratio of gels in NS systems, which is more susceptible to decalcification than the gels in NH systems [43]. The latter is due to the presence of a higher concentration of Ca in the pore solution [7], which contributes to the formation of calcium carbonate and the densification of microstructure [6,41]. Additionally, as shown in Fig. 12A, the increments in compressive strength of NH mortars upon carbonation are comparable under different conditions. As shown in Fig. 12B, the reduction in compressive strength of NS mortars under fog and water conditions is larger than the others, which is probably due to the problem of leaching.

3.8. Summary

Based on the experimental results of this study, a summary of the performances of AASM under different curing conditions is shown in Fig. 13, considering both the magnitudes and trends. It should be noted

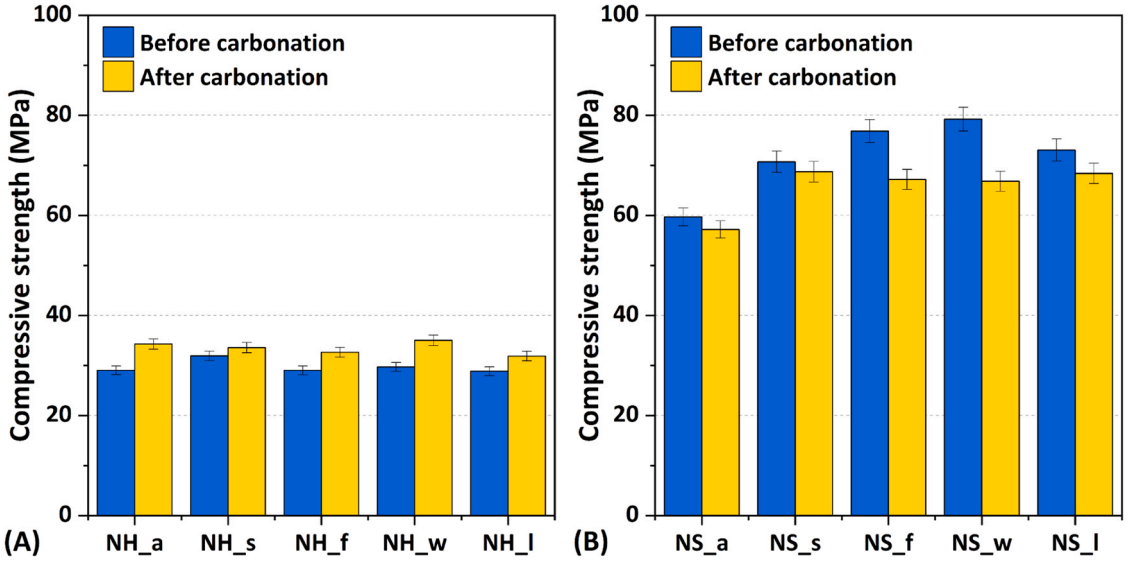

Fig. 12. Compressive strength of 28 d AASM before and after 28 days of accelerated carbonation.

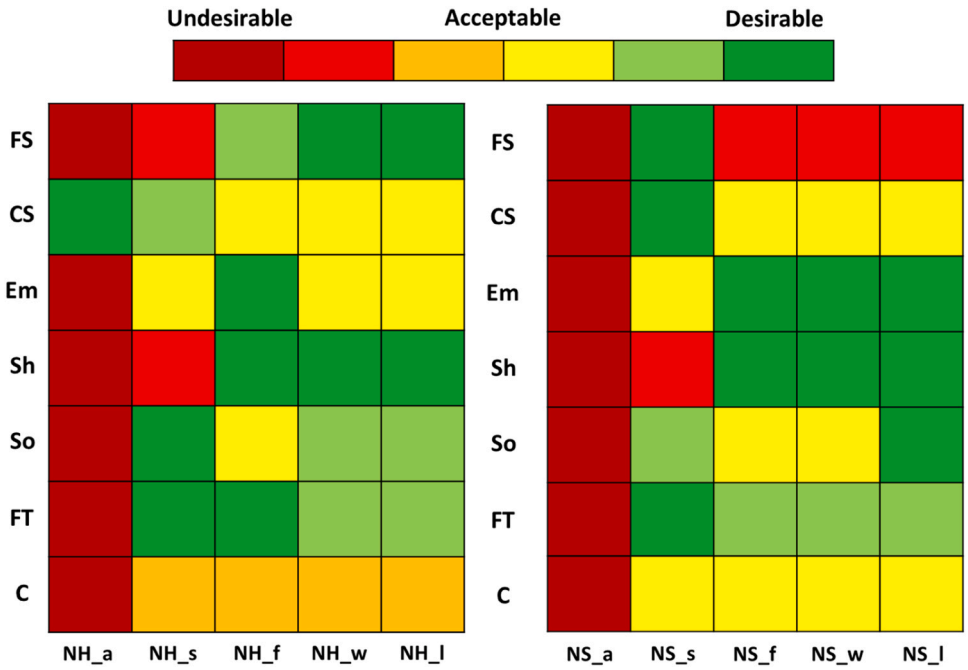

Fig. 13. A comparative analysis of mechanical properties, volume stability, and durability of AASM cured under various conditions. "FS", "CS", "Em", "Sh", "So", "FT" and "C" refer to flexural strength, compressive strength, elastic modulus, shrinkage, sorptivity, freeze-thaw and carbonation tests, respectively. The NH and NS mortars are evaluated individually.

that the NH and NS mortars are assessed individually.

The mechanical properties, volume stability and durability of both NH and NS AASM are unsatisfactory under ambient conditions, except for the compressive strength of NH mortar. Compared with sealed and high-humidity conditions, their impacts on the properties of AASM are different due to the use of different activators. High-humidity conditions are detrimental to the flexural strength of NS samples but are advantageous for that of NH samples. Due to the problem of leaching, both NH and NS mortars show lower compressive strength than those under sealed conditions. Therefore, a long-term high-humidity curing is undesirable. The result of elastic modulus is more related to compressive strength. The elastic moduli of AASM under sealed and high-humidity conditions are comparable, which are much higher than those under ambient conditions. High-humidity conditions can efficiently mitigate the shrinkage of both NH and NS mortars, while sealed mortars show relatively large magnitudes, especially for NS ones. As for the sorptivity, freeze-thaw and carbonation, the results of these measurements are generally dependent on the surface properties. The samples under ambient and high-humidity conditions might be more vulnerable to cracking than those under sealed conditions due to the constantly dry conditions and the large humidity gradient between samples and environments during preconditioning. Limewater curing shows limited advantages in the enhancement of mechanical properties and durability of AASM.

To sum up, ambient conditions result in undesirable mechanical properties and durability of AASM. Hence, it is crucial to strictly avoid drying during the curing period. Overall, sealed curing can deliver satisfactory long-term performances to AASM, but it does induce relatively large autogenous shrinkage. This substantial shrinkage can be effectively suppressed by high-humidity curings, but prolonged exposure to such circumstances may result in leaching problems and undesirable reductions in long-term mechanical properties and durabilities. Therefore, we recommend maintaining high-humidity conditions for AAS materials during initial periods, for instance by using wet cloth covering, which can not only provide high humidity conditions but also prevent leaching problems at early ages. Then, if possible, sealing the products before service is advisable. This protocol can not only effectively reduce the large early-age shrinkage of AAS materials without significant leaching but also contribute to delivering a good development of long-term mechanical properties and durability.

4. Conclusions

In this study, the effects of curing regimes on the mechanical properties, volume stability and durability of AASM are investigated and the mechanisms behind them are revealed. The conclusions can be summarized as follows:

1. Generally, sealed curing is beneficial for the development of mechanical properties of AASM, while ambient curing shows the most undesirable properties, especially concerning the decreasing trends of flexural strength and elastic modulus. High-humidity curings are favourable for enhancing the flexural strength of NH mortars but are detrimental to the NS ones. NH mortars show the highest compressive strength under ambient conditions, under which the NS mortars show the lowest. Both NH and NS mortars under high-humidity conditions show lower long-term compressive strength than those under sealed conditions.
2. The NS mortar has low porosity, accompanied by considerably larger shrinkage than that of the NH one. This shrinkage is further exacerbated by drying and carbonation under ambient conditions, leading to the formation and propagation of surface cracks. The AASM shows large shrinkage under sealed conditions, which can be effectively suppressed by high-humidity curings.
3. AASM cured under ambient conditions has higher water sorptivity than that under other curing regimes. Compared with the sealed regime, high-humidity curings result in the problem of leaching, which can deteriorate the pore structure and increase the sorptivity of the mortar. Saturated limewater curing is conducive to the reduction in water sorptivity, particularly for NS-activated mortars.
4. The sorptivity results are correlated with the freeze-thaw and carbonation tests, as they are all dependent on the surface properties of AASM. The mortars exposed to ambient conditions show the highest water sorptivity, and thereby exhibit the poorest resistance

to freeze-thaw cycles and carbonation. Both the exposed and upper sides of the NH mortars show significant damage following freeze-thaw cycles. The carbonation depth of AASM depends on the process of preconditioning. The carbonation rates of AASM during accelerated carbonation are comparable, which indicates that different curing conditions can only affect the external part of the mortars.

5. Based on the experimental results, an optimal curing protocol for AASM might be a high-humidity condition (e.g. wet cloth covering) at early ages, followed by sealed curing. This approach can not only reduce the significant early shrinkage but also contribute to desirable long-term mechanical properties and durability without leaching.

CRediT authorship contribution statement

Guang Ye: Writing – review & editing, Supervision, Funding acquisition. **Haoming Wu:** Methodology, Investigation. **Chen Liu:** Writing – original draft, Methodology, Investigation, Conceptualization. **Hu Shi:** Investigation. **Zhenming Li:** Writing – review & editing, Supervision.

Declaration of Competing Interest

The authors declare that they have no known competing financial interests or personal relationships that could have appeared to influence the work reported in this paper.

Data availability

The data that has been used is confidential.

Acknowledgements

Chen Liu would like to acknowledge the funding supported by the China Scholarship Council (CSC) under grant No. 201906950102. This work is also supported by the Guangdong Provincial Key Laboratory of Intelligent and Resilient Structures for Civil Engineering (2023B1212010004).

Appendix

Fig. A1 shows the relative humidity (RH) of NS mortars. This test aims to monitor the change of RH in the sample under sealed conditions. The experiment was measured by a Rotronic hygroscopic DT station equipped with HC2-AW measuring cells. The sensors were calibrated by four oversaturated chemical solutions (NaCl, KCl, KNO_3 and K_2SO_4) before measurement, with a RH range from 75 % to 98 % at 20 °C. Two replicates were carried out for each sample. It is observed that the RH of NS mortars under sealed conditions decreases from 95 % to 78 %.

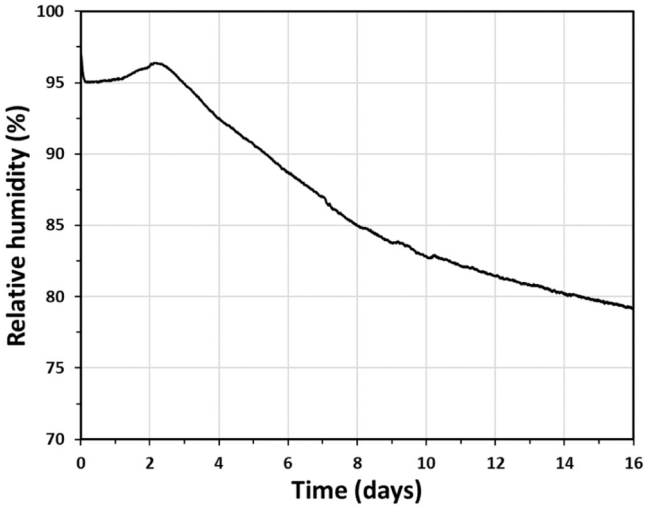

Fig. A1. Relative humidity of NS mortars under sealed conditions.

Fig. A2 shows the appearance of NS mortars exposed to ambient conditions for 7 d. The microcracks can be observed on the surface of samples, attributed to the dry shrinkage.

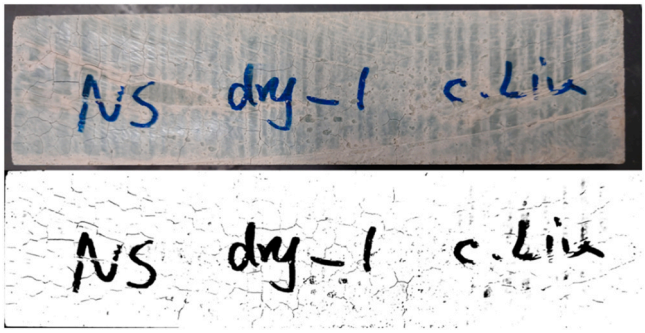

Fig. A2. Appearance of the surface cracks of NS mortars exposed to ambient conditions for 7 d.

References

[1] J.L. Provis, Alkali-activated materials, Cem. Concr. Res. 114 (2018) 40–48, https://doi.org/10.1016/j.cemconres.2017.02.009.

[2] J.L. Provis, A. Palomo, C. Shi, Advances in understanding alkali-activated materials, Cem. Concr. Res. 78 (2015) 110–125, https://doi.org/10.1016/j.cemconres.2015.04.013.

[3] C. Shi, A.F. Jiménez, A. Palomo, New cements for the 21st century: the pursuit of an alternative to Portland cement, Cem. Concr. Res. 41 (2011) 750–763, https://doi.org/10.1016/j.cemconres.2011.03.016.

[4] Z. Li, T. Lu, X. Liang, H. Dong, G. Ye, Mechanisms of autogenous shrinkage of alkali-activated slag and fly ash pastes, Cem. Concr. Res. 135 (2020) 106107, https://doi.org/10.1016/j.cemconres.2020.106107.

[5] S.A. Bernal, R. San Nicolas, J.L. Provis, R. Mejía De Gutiérrez, J.S.J. Van Deventer, Natural carbonation of aged alkali-activated slag concretes, Mater. Struct. Constr. 47 (2014) 693–707, https://doi.org/10.1617/s11527-013-0089-2.

[6] S.A. Bernal, R.M. de Gutierrez, J.L. Provis, V. Rose, Effect of silicate modulus and metakaolin incorporation on the carbonation of alkali silicate-activated slags, Cem. Concr. Res. 40 (2010) 898–907, https://doi.org/10.1016/j.cemconres.2010.02.003.

[7] C. Liu, X. Liang, Y. Chen, Z. Li, G. Ye, Degradation of alkali-activated slag subject to water immersion, Cem. Concr. Compos. 142 (2022), https://doi.org/10.1016/j.cemconcomp.2023.105157.

[8] Z. Zhang, J.L. Provis, X. Ma, A. Reid, H. Wang, Efflorescence and subflorescence induced microstructural and mechanical evolution in fly ash-based geopolymers, Cem. Concr. Compos. 92 (2018) 165–177, https://doi.org/10.1016/j.cemconcomp.2018.06.010.

[9] E. Najafi Kani, A. Allahverdi, J.L. Provis, Efflorescence control in geopolymer binders based on natural pozzolan, Cem. Concr. Compos. 34 (2012) 25–33, https://doi.org/10.1016/j.cemconcomp.2011.07.007.

[10] Z. Li, M. Nedeljković, B. Chen, G. Ye, Mitigating the autogenous shrinkage of alkali-activated slag by metakaolin, Cem. Concr. Res. 122 (2019) 30–41, https://doi.org/10.1016/j.cemconres.2019.04.016.

[11] S.A. Bernal, R. San Nicolas, R.J. Myers, R. Mejía De Gutiérrez, F. Puertas, J.S.J. Van Deventer, J.L. Provis, MgO content of slag controls phase evolution and structural changes induced by accelerated carbonation in alkali-activated binders, Cem. Concr. Res. 57 (2014) 33–43, https://doi.org/10.1016/j.cemconres.2013.12.003.

[12] V.S. Athira, A. Bahurudeen, M. Saljas, K. Jayachandran, Influence of different curing methods on mechanical and durability properties of alkali activated binders, Constr. Build. Mater. 299 (2021) 123963, https://doi.org/10.1016/j.conbuildmat.2021.123963.

[13] M. Nodehi, T. Ozbakkaloglu, A. Gholampour, T. Mohammed, X. Shi, The effect of curing regimes on physico-mechanical, microstructural and durability properties of alkali-activated materials: A review, Constr. Build. Mater. 321 (2022) 126335, https://doi.org/10.1016/j.conbuildmat.2022.126335.

[14] S.-D. Wang, K.L. Scrivener, P.L. Pratt, Factors affecting the strength of alkali-activated slag, Cem. Concr. Res. 24 (1994) 1033–1043, https://doi.org/10.1016/0008-8846(94)90026-4.

[15] F. Collins, J.G. Sanjayan, Microcracking and strength development of alkali activated slag concrete, Cem. Concr. Compos. 23 (2001) 345–352, https://doi.org/10.1016/S0958-9465(01)00003-8.

[16] M. Rostami, K. Behfarnia, The effect of silica fume on durability of alkali activated slag concrete, Constr. Build. Mater. 134 (2017) 262–268, https://doi.org/10.1016/j.conbuildmat.2016.12.072.

[17] M. Chi, Effects of dosage of alkali-activated solution and curing conditions on the properties and durability of alkali-activated slag concrete, Constr. Build. Mater. 35 (2012) 240–245, https://doi.org/10.1016/j.conbuildmat.2012.04.005.

[18] E. Altan, S.T. Erdoğan, Alkali activation of a slag at ambient and elevated temperatures, Cem. Concr. Compos. 34 (2012) 131–139.

[19] T. Bakharev, J.G. Sanjayan, Y.-B. Cheng, Effect of elevated temperature curing on properties of alkali-activated slag concrete, Cem. Concr. Res. 29 (1999) 1619–1625.

[20] O.Y. Bayraktar, A. Benli, B. Bodur, A. Öz, G. Kaplan, Performance assessment and cost analysis of slag/metakaolin based rubberized semi-lightweight geopolymers with perlite aggregate: sustainable reuse of waste tires, Constr. Build. Mater. 411 (2024) 1–18, https://doi.org/10.1016/j.conbuildmat.2023.134655.

[21] Rathore, Shivendra Singh, and Chakradhara Rao Meesala. "Influence of recycled coarse aggregate on properties of fly ash and slag-based geopolymer concrete cured under oven and ambient temperature." *World Journal of Engineering* (2024).

[22] X. Yao, T. Yang, Z.Z. Zhang, Y. Wang, X. Liu, W.D. Zhang, Z. Li, Y. Zhang, Y. Li, Y. Ren, K. Sun, X. Peng, S. Wang, L. Zeng, P. Ran, G. Ji, M.A. Longhi, E. D. Rodríguez, B. Walkley, Z.Z. Zhang, A.P. Kirchheim, S.P. Kang, S.J. Kwon, X. Xue, Y.L. Liu, J.G. Dai, C.S. Poon, W.D. Zhang, P. Zhang, Z.Z. Zhang, J.L. Provis, X. Ma, A. Reid, H. Wang, J.L. Provis, A. Reid, X. Yao, T. Yang, Z.Z. Zhang, J.L. Provis, A. Reid, H. Wang, R.R. Lloyd, J.L. Provis, J.S.J. Van Deventer, Compressive strength development and shrinkage of alkali-activated fly ash–slag blends associated with efflorescence, Mater. Struct. 49 (2016) 165–177, https://doi.org/10.1016/j.cemconcomp.2018.06.010.

[23] M. Dong, M. Elchalakani, A. Karrech, Curing conditions of alkali-activated fly ash and slag mortar, J. Mater. Civ. Eng. 32 (2020) 4020122, https://doi.org/10.1061/(ASCE)MT.1943-5533.0003233.

[24] H. El-Hassan, E. Shehab, A. Al-Sallamin, Influence of different curing regimes on the performance and microstructure of alkali-activated slag concrete, J. Mater. Civ. Eng. 30 (2018) 04018230, https://doi.org/10.1061/(asce)mt.1943-5533.0002436.

[25] B.S. En, Methods of testing cement—Part 1: determination of strength, Eur. Comm. Stand. 169 (2005) 36. Brussels, Belgium.

[26] European committee for standardization. NEN-EN 196-1. Methods of testing cement - Part 1: Determination of strength. 2016., (n.d.).

[27] A.S. for T. and M.C.C.-1 on Cement, Standard Test Method for Drying Shrinkage of Mortar Containing Hydraulic Cement, ASTM International, 2010.

[28] C. Liu, Y. Liu, Z. Liu, C. Hu, X. Huang, L. Yang, F. Wang, Heat-cured concrete: improving the early strength and pore structure by activating aluminosilicate internal curing agent with triisopropanolamine, J. Am. Ceram. Soc. 102 (2019) 6227–6238, https://doi.org/10.1111/jace.16458.

[29] C. Liu, L. Yang, Z. Li, S. Nie, C. Hu, F. Wang, Improve the long-term property of heat-cured mortars blended with fly ash by internal curing, J. Build. Eng. 54 (2022) 104624, https://doi.org/10.1016/j.jobe.2022.104624.

[30] C. Liu, L. Yang, F. Wang, S. Hu, Enhance the durability of heat-cured mortars by internal curing and pozzolanic activity of lightweight fine aggregates, Constr. Build. Mater. 270 (2021) 121439, https://doi.org/10.1016/j.conbuildmat.2020.121439.

[31] Prathamesh Pawar, Sudhir Patil, Sathe Sandeep, Exploring the impact of red mud on the mechanical, durability, and microstructure properties of concrete, World Journal of Engineering (2024).

[32] ASTM C1585-13, Standard test method for measurement of rate of absorption of water by hydraulic cement concretes, ASTM Int. 41 (2013) 1–6.

[33] F. Winnefeld, G.J.G. Gluth, S.A. Bernal, M.C. Bignozzi, L. Carabba, S. Chithiraputhiran, A. Dehghan, S. Dolenec, K. Dombrowski-Daube, A. Dubey, V. Ducman, Y. Jin, K. Peterson, D. Stephan, J.L. Provis, RILEM TC 247-DTA round robin test: sulfate resistance, alkali-silica reaction and freeze–thaw resistance of alkali-activated concretes, Mater. Struct. Constr. 53 (2020) 1–17, https://doi.org/10.1617/s11527-020-01562-0.

[34] S.A. Bernal, J.L. Provis, B. Walkley, R. San Nicolas, J.D. Gehman, D.G. Brice, A. R. Kilcullen, P. Duxson, J.S.J. Van Deventer, Gel nanostructure in alkali-activated binders based on slag and fly ash, and effects of accelerated carbonation, Cem. Concr. Res. 53 (2013) 127–144, https://doi.org/10.1016/j.cemconres.2013.06.007.

[35] M. Ben Haha, G. Le Saout, F. Winnefeld, B. Lothenbach, Influence of activator type on hydration kinetics, hydrate assemblage and microstructural development of alkali activated blast-furnace slags, Cem. Concr. Res. 41 (2011) 301–310, https://doi.org/10.1016/j.cemconres.2010.11.016.

[36] H. Ye, A. Radlińska, Shrinkage mechanisms of alkali-activated slag, Cem. Concr. Res. 88 (2016) 126–135, https://doi.org/10.1016/j.cemconres.2016.07.001.

[37] C. Liu, J. Xie, Z. Li, G. Ye, Cracking mechanisms of alkali-activated slag pastes subjected to water immersion: an experimental and numerical study, (n.d.).

[38] M.H. Hubler, J.J. Thomas, H.M. Jennings, Influence of nucleation seeding on the hydration kinetics and compressive strength of alkali activated slag paste, Cem. Concr. Res. 41 (2011) 842–846, https://doi.org/10.1016/j.cemconres.2011.04.002.

[39] P. Termkhajornkit, T. Nawa, K. Kurumisawa, Effect of water curing conditions on the hydration degree and compressive strengths of fly ash-cement paste, Cem. Concr. Compos. 28 (2006) 781–789, https://doi.org/10.1016/j.cemconcomp.2006.05.018.

[40] G. Huang, Y. Ji, L. Zhang, J. Li, Z. Hou, The influence of curing methods on the strength of MSWI bottom ash-based alkali-activated mortars: the role of leaching of OH− and free alkali, Constr. Build. Mater. 186 (2018) 978–985, https://doi.org/10.1016/j.conbuildmat.2018.07.224.

[41] Z. Shi, C. Shi, S. Wan, N. Li, Z. Zhang, Effect of alkali dosage and silicate modulus on carbonation of alkali-activated slag mortars, Cem. Concr. Res. 113 (2018) 55–64, https://doi.org/10.1016/j.cemconres.2018.07.005.

[42] A. Morandeau, M. Thiéry, P. Dangla, Investigation of the carbonation mechanism of CH and C-S-H in terms of kinetics, microstructure changes and moisture properties, Cem. Concr. Res. 56 (2014) 153–170, https://doi.org/10.1016/j.cemconres.2013.11.015.

[43] N. Li, N. Farzadnia, C. Shi, Microstructural changes in alkali-activated slag mortars induced by accelerated carbonation, Cem. Concr. Res. 100 (2017) 214–226, https://doi.org/10.1016/j.cemconres.2017.07.008.

[44] D. Le Cornec, Q. Wang, L. Galoisy, G. Renaudin, L. Izoret, G. Calas, Greening effect in slag cement materials, Cem. Concr. Compos. 84 (2017) 93–98, https://doi.org/10.1016/j.cemconcomp.2017.08.017.

[45] M. Chaouche, X.X. Gao, M. Cyr, M. Cotte, L. Frouin, On the origin of the blue/green color of blast-furnace slag-based materials: sulfur K-edge XANES investigation, J. Am. Ceram. Soc. 100 (2017) 1707–1716, https://doi.org/10.1111/jace.14670.

[46] Y.F. Houst, F.H. Wittmann, Influence of porosity and water content on the diffusivity of CO [sub 2] and O [sub 2] through hydrated cement paste, (1994).

[47] Y. Ding, J.G. Dai, C.J. Shi, Mechanical properties of alkali-activated concrete: a state-of-the-art review, Constr. Build. Mater. 127 (2016) 68–79, https://doi.org/10.1016/j.conbuildmat.2016.09.121.

[48] Z. Li, S. Zhang, X. Liang, G. Ye, Cracking potential of alkali-activated slag and fly ash concrete subjected to restrained autogenous shrinkage, Cem. Concr. Compos. 114 (2020) 103767, https://doi.org/10.1016/j.cemconcomp.2020.103767.

[49] C. Liu, Z. Li, S. Nie, S. Skibsted, G. Ye, Structural evolution of calcium sodium aluminosilicate hydrate (C-(N-)A-S-H) gels induced by water exposure: the impact of Na leaching, Cem. Concr. Res. 178 (2024), https://doi.org/10.1016/j.cemconres.2024.107432.

[50] C. Liu, Y. Zhang, Z. Li, G. Ye, Underwater carbonation of alkali-activated slag paste, (2024).

[51] R. Wang, Z. Hu, Y. Li, K. Wang, H. Zhang, Review on the deterioration and approaches to enhance the durability of concrete in the freeze–thaw environment,

Constr. Build. Mater. 321 (2022) 126371, https://doi.org/10.1016/j.conbuildmat.2022.126371.
[52] M.J. Setzer, Draft recommendation for test method for the freeze-thaw resistance of concrete Tests with water (CF) or with sodium chloride solution (CDF), Mater. Struct. 28 (1995) 175–182, https://doi.org/10.1007/BF02473223.
[53] F. Puertas, M. Palacios, T. Vázquez, Carbonation process of alkali-activated slag mortars, J. Mater. Sci. 41 (2006) 3071–3082, https://doi.org/10.1007/s10853-005-1821-2.
[54] T. Bakharev, J.G. Sanjayan, Y.B. Cheng, Resistance of alkali-activated slag concrete to carbonation, Cem. Concr. Res. 31 (2001) 1277–1283, https://doi.org/10.1016/S0008-8846(01)00574-9.